Ultra-wide bandgap, conductive, high mobility, and high quality melt-grown bulk ZnGa$_2$O$_4$ single crystals

Zbigniew Galazka, Steffen Ganschow, Robert Schewski, et al.

COLLECTIONS

Paper published as part of the special topic on Wide Bandgap Oxides

ARTICLES YOU MAY BE INTERESTED IN

A review of Ga$_2$O$_3$ materials, processing, and devices
Applied Physics Reviews **5**, 011301 (2018); https://doi.org/10.1063/1.5006941

MOCVD grown epitaxial β-Ga$_2$O$_3$ thin film with an electron mobility of 176 cm^2/V s at room temperature
APL Materials **7**, 022506 (2019); https://doi.org/10.1063/1.5058059

Perspective: Ga$_2$O$_3$ for ultra-high power rectifiers and MOSFETS
Journal of Applied Physics **124**, 220901 (2018); https://doi.org/10.1063/1.5062841

Ultra-wide bandgap, conductive, high mobility, and high quality melt-grown bulk ZnGa$_2$O$_4$ single crystals

Zbigniew Galazka,[a] 🆔 Steffen Ganschow, Robert Schewski, 🆔 Klaus Irmscher, 🆔 Detlef Klimm, 🆔
Albert Kwasniewski, Mike Pietsch, Andreas Fiedler, Isabelle Schulze-Jonack, Martin Albrecht, 🆔
Thomas Schröder, and Matthias Bickermann 🆔

AFFILIATIONS

Leibniz Institute for Crystal Growth, Max-Born-Str. 2, 12489 Berlin, Germany

[a] Author to whom correspondence should be addressed: zbigniew.galazka@ikz-berlin.de

ABSTRACT

Truly bulk ZnGa$_2$O$_4$ single crystals were obtained directly from the melt. High melting point of 1900 ± 20 °C and highly incongruent evaporation of the Zn- and Ga-containing species impose restrictions on growth conditions. The obtained crystals are characterized by a stoichiometric or near-stoichiometric composition with a normal spinel structure at room temperature and by a narrow full width at half maximum of the rocking curve of the 400 peak of (100)-oriented samples of 23 arcsec. ZnGa$_2$O$_4$ is a single crystalline spinel phase with the Ga/Zn atomic ratio up to about 2.17. Melt-grown ZnGa$_2$O$_4$ single crystals are thermally stable up to 1100 and 700 °C when subjected to annealing for 10 h in oxidizing and reducing atmospheres, respectively. The obtained ZnGa$_2$O$_4$ single crystals were either electrical insulators or n-type semiconductors/degenerate semiconductors depending on growth conditions and starting material composition. The as-grown semiconducting crystals had the resistivity, free electron concentration, and maximum Hall mobility of 0.002–0.1 Ωcm, 3×10^{18}–9×10^{19} cm^{-3}, and 107 cm^2 V^{-1} s^{-1}, respectively. The semiconducting crystals could be switched into the electrically insulating state by annealing in the presence of oxygen at temperatures ≥700 °C for at least several hours. The optical absorption edge is steep and originates at 275 nm, followed by full transparency in the visible and near infrared spectral regions. The optical bandgap gathered from the absorption coefficient is direct with a value of about 4.6 eV, close to that of β-Ga$_2$O$_3$. Additionally, with a lattice constant of a = 8.3336 Å, ZnGa$_2$O$_4$ may serve as a good lattice-matched substrate for magnetic Fe-based spinel films.

Transparent semiconducting/conducting oxides (TSOs/TCOs) constitute a continuously growing area of fundamental research and applications[1–5] as they offer transparency in the visible spectrum and semiconducting behavior. A combination of these features offers applications in electronics, optoelectronics, sensing systems, and photovoltaics. The main focus has been directed to binary systems, such as ZnO, β-Ga$_2$O$_3$, In$_2$O$_3$, and SnO$_2$ revealing wide and ultra-wide bandgaps ranging from ~2.7 eV for In$_2$O$_3$[6] to ~4.85 eV for β-Ga$_2$O$_3$.[7] An important factor in the research of the binary systems was the availability of bulk crystals [in spite of their thermal instability at high temperatures and high melting points (MPs) ≥1800 °C] that enable to probe properties of high structural quality materials and use them as substrates for epitaxial growth and devices. In addition to binary systems, there is also a search for ternary systems (e.g., In$_2$O$_3$-SnO$_2$ and BaSnO$_3$). The ternary and quaternary systems have the advantage of two or three cation sites enabling higher degree of freedom for doping, but also suffer from incongruent decomposition when grown from the melt, that creates challenging tasks for obtaining bulk single crystals of a reasonable size.

An example of ternary systems that may offer an ultra-wide energy gap and semiconducting behavior relates to Ga-based spinels with the general formula of MeGa$_2$O$_4$, where Me is a divalent metal. We already demonstrated semiconducting behavior of bulk MgGa$_2$O$_4$ crystals having an ultra-wide energy gap of 4.9 eV; however, the carrier mobility was rather low. Another spinel that would reveal good electrical properties and ultra-wide energy gap is ZnGa$_2$O$_4$ (zinc gallate), which is the focus of the present research. ZnGa$_2$O$_4$ is cubic (Fd$\bar{3}$m space group) with a normal spinel structure in which Zn^{2+} and Ga^{3+} cations are distributed in tetrahedral and octahedral lattice sites, respectively. The lattice parameter is 8.3342 Å.[8]

ZnGa$_2$O$_4$ has been found as a long-lasting, low-voltage cathodoluminescence phosphor that can be used in vacuum fluorescent and field emission displays. It shows a strong blue emission (intrinsic) when undoped[9] and green to red emissions when doped with Mn,[10] Eu,[11] or Cr.[12] Moreover, the luminescence could be tuned in the whole visible spectrum by double (Mn + Cr),[13] (Eu + Tb),[14] or even triple (Ge + Li + Mn)[15] co-doping. The phosphors can be used in electroluminescent devices.[10,16] Other demonstrated devices include a photodetector,[17] a photocatalyst,[18] a gas sensor,[19] and a MOSFET.[20] ZnGa$_2$O$_4$ is typically prepared as ceramic,[21] nano-structures,[17] or layers prepared by sol-gel,[22–24] RF magnetron sputtering,[25–30] pulsed laser deposition,[31–37] metalorganic chemical vapor deposition (MOCVD),[38] and mist-CVD.[39] The films/layers are grown heteroepitaxially as no ZnGa$_2$O$_4$ substrates are available. As the result, they are either amorphous or polycrystalline, which significantly affects optical and electrical properties.

There were also attempts to obtain bulk ZnGa$_2$O$_4$ crystals. So far, small bulk crystals were demonstrated by the flux method only at growth temperatures below 1300 °C: Chase and Osmer[40] (Bi$_2$O$_3$ or PbO–PbF$_2$–B$_2$O$_3$), Van Der Straten et al.[41] (PbO-PbF$_2$-B$_2$O$_3$-SiO$_2$, Pb$_2$P$_2$O$_7$), and Yan et al.[42,43] (PbO-B$_2$O$_3$). At optimized flux composition and growth conditions, the obtained crystals were substantially stoichiometric and colourless, with the largest dimension along one edge up to 10 mm.[42] Crystalline ZnGa$_2$O$_4$ fibres were also mentioned by Jia et al.[44] obtained by the Laser Heated Pedestal Growth (LHPG) method. However, due to an intensive evaporation of Zn, the growth of fibres ended fast.

Although optical properties, especially luminescence, of ZnGa$_2$O$_4$ were intensively studied, little is known about electrical properties. In fact, the obtained materials were typically electrically insulating or exhibited very poor electrical properties, likely due to very poor structural quality. For example, heteroepitaxial films obtained by MOCVD revealed a free electron concentration, resistivity, and electron mobility of 1.9 × 10^{14}–6.7 × 10^{16} cm^{-3}, 68 − 5.7 × 10^3 Ωcm, and 1.4–5.8 cm^2 V^{-1} s^{-1}, respectively.[38] Ceramics annealed in a hydrogen-containing atmosphere showed electrical conduction with a resistivity of about 0.03 Ωcm at room temperature (RT), which was basically constant versus temperature below RT that indicates a degenerate state.[45] Flux-grown crystals were electrically insulating, but after annealing in the presence of hydrogen, the outer surface became conducting with the resistivity of about 10 Ωcm at RT.[43]

An objective of this report is to demonstrate truly bulk ZnGa$_2$O$_4$ single crystals of high structural perfection obtained directly from the melt for the first time, which enable substrate preparation for epitaxial growth and devices. Another objective is to provide basic structural, chemical, electrical, and optical characterization of the melt-grown ZnGa$_2$O$_4$ single crystals, which may contribute to better understanding of the material properties, in particular its electrical properties.

Thermodynamic calculations were carried out using the FactSage software package[46] to get information on the activity of the species relevant for melt growth of ZnGa$_2$O$_4$.

Thermal analysis was carried out by thermogravimetry (TG) and simultaneous differential thermal analysis (DTA) up to 1620 °C in oxygen with the Netzsch type STA 449 C and STA 409 CD equipment using the Pt sample and reference crucibles.

ZnGa$_2$O$_4$ crystals were grown from the melt by the vertical gradient freeze (VGF) and the Czochralski methods. The growth furnace included an iridium crucible of 4 cm diameter, a thermal insulation surrounding the crucible from all sides, and an RF coil for inductive heating of the crucible. More details on growth experiments are given below.

The chemical composition of the grown single crystals was determined by X-ray fluorescence (XRF) from Bruker and an inductively coupled plasma-optical emission spectrometer (ICP-OES) from Thermo Fisher Scientific. The milled crystal samples were digested in 2 ml HCl + 1 ml HNO$_3$ + 1.7 ml H$_2$O at 200 °C for 20 min. The chemical composition was also checked by X-ray fluorescence analysis using a Bruker Tornado M4 spectrometer with a Rh tube operated at 50 kV and 200 μA equipped with a polycapillary lens focussing the exciting beam to a spot size of approximately 25 μm. Fluorescence spectra were recorded with a Si drift detector. Element concentrations were obtained using a standardless fundamental parameter model quantification.

The real structure of the crystals was evaluated by using several techniques: (i) X-ray powder diffraction (XRD) using a diffractometer system XRD 3003 PTS (GE Inspection Technologies) was applied to ascertain whether phase purity prevails. (ii) Rocking curves were measured using a high resolution X-ray diffractometer system HR XRD Master (Seifert) equipped with a Bartels monochromator Ge(220) and choosing an aperture of 2 × 10 mm^2 to check for curve broadening caused by extended defects. (iii) Etch pits were counted that had developed after wet etching of an as-grown (100) crystal face in NaOH at 100 °C for 1 h or by dry etching at 1400 °C in air for 10 h. (iv) Transmission electron microscopy (TEM) has been performed with a spherical aberration corrected FEI Titan 80-300 operating at 300 kV and equipped with a highly brilliant cathode (X-FEG).

Thermal conductivity was measured with the laser flash technique using an LFA 427 from Netzsch. Sample slices with ca. 0.75 mm thickness were covered on the bottom and top sides with graphite spray to increase infrared absorption and emission of a Nd:YAG laser pulse (duration 0.8 ms) that irradiated the bottom surface. The thermal signal at the top surface was measured by an InSb detector (cooled with liquid nitrogen) and analyzed for thermal diffusivity with Mehling's model[47] for semi-transparent media. By multiplying the thermal diffusivity with the mass density $\rho = 6.17$ g/cm^3[48] and the temperature-dependent specific heat capacity that was estimated from the literature data for ZnO and Ga$_2$O$_3$,[46] the thermal conductivity was derived. Typically three laser shots were performed for every temperature step, which was either 50 or 20 K.

Electrical conductivity and Hall effect of the crystals were measured in van-der-Pauw configuration at room temperature using a Hall measurement system HMS 7504 (Lake Shore). The contacts were prepared by rubbing a little In-Ga eutectic mixture at four points on the sample rim of wafer-shaped samples of about 25 mm^2 area and 0.5 mm thickness. Ohmic behavior of these contacts was accomplished by discharging a capacitor over each two contacts. Electrical set-up and sample dimensions limited resistivity measurements to values up to about 10^8 Ωcm. Therefore, samples with higher resistivity could not be measured and are indicated as electrical insulators. Electron concentration and mobility were calculated under the assumption of a unity Hall scattering factor.

Optical transmittance spectra were recorded at room temperature using a spectrophotometer Lambda 19 (PerkinElmer). Double side polished samples of thicknesses between 500 μm and 250 μm were prepared for these measurements. In particular for the measurement of the fundamental absorption edge, the thinnest sample, an aperture of 4 mm diameter, and reference beam attenuation to 1% were used. For the other transmission measurements, an integrating sphere was employed to minimize scattering losses. Absorption coefficients were calculated from the transmittance data by approximately taking account of the reflection losses (see, e.g., Ref. 49) setting the refraction index to 2.

A starting material for crystal growth of ZnGa$_2$O$_4$ is formed from a mixture of dried, pressed, and sintered ZnO and Ga$_2$O$_3$ powders. Both oxides are thermally unstable at high temperatures and tend to decompose even before solid state synthesis. The partial pressures p(Zn) and p(Ga$_2$O) of the most volatile species Zn(g) and Ga$_2$O(g) (g stands for the gas phase), respectively, versus temperature at low (2%) and high (100%) oxygen partial pressures are shown in Fig. 1. At melting point (MP) of ZnGa$_2$O$_4$, which we measured at 1900 $\pm$ 20 °C, p(Zn) is more than 2000 times higher than p(Ga$_2$O). This leads to an incongruent evaporation, which is time and temperature gradient dependent, and consequently leads to a shift toward Ga-rich composition, even at high oxygen concentrations, due to much higher Zn losses as compared to Ga losses.
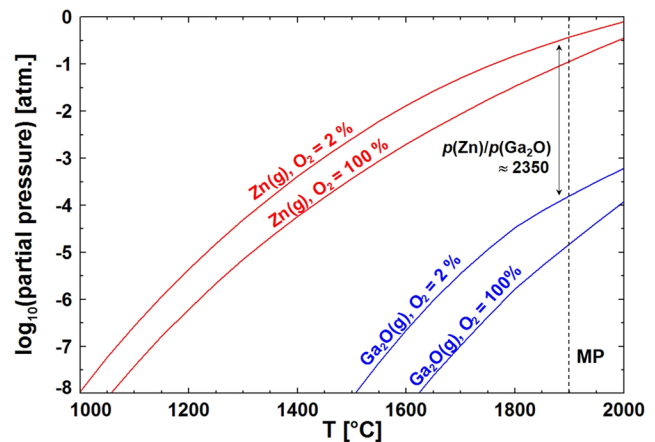

FIG. 1. Zn(g) and Ga$_2$O(g) partial pressure in the ZnO-Ga$_2$O$_3$ system vs. temperature at low (2%) and high (100%) oxygen partial pressure.

The growth experiments were performed in 40 mm diameter Ir crucibles (with either flat or conical bottoms) inductively heated with an RF coil. The growth furnace was located within a growth chamber enabling a variable growth atmosphere and pressure. The growth atmosphere consisted of Ar + O$_2$ with an O$_2$ concentration between 8 and 40 vol. % of the total gas flow, while the total pressure within the growth chamber was either 1, 2, or 10 bars. High oxygen concentration in a combination with Ir was possible by applying a new oxygen delivery scheme to the growth furnace as we developed for bulk β-Ga$_2$O$_3$ single crystals grown by the Czochralski method.[50] The composition of the starting material was Zn$_{1+x}$Ga$_2$O$_4$, where x = 0–0.04. The excess of ZnO in the starting material aimed to compensate Zn losses that are much higher than Ga losses. Both powders ZnO (5N) and Ga$_2$O$_3$ (5N) were first dried in ambient air for 10 h at 600 and 800 °C, respectively, then mixed, pressed at 2000 bars, and sintered at 600 °C for 10 h. Intentional doping with Si^{4+} and Zr^{4+} ions was practiced as well.

Due to highly incongruent decomposition and evaporation of the ZnO-Ga$_2$O$_3$ system even at high oxygen concentrations, it is clear that keeping the system in the liquid phase for an extended time will change the composition significantly, leading to a stoichiometry deviation and consequently to a second phase formation. In the present growth experiments, the dwell time of the ZnO-Ga$_2$O$_3$ system in the liquid phase that led to single crystalline formation did not exceed 5 h. Three methods were applied to grow ZnGa$_2$O$_4$ single crystals from the melt: the vertical gradient freeze (VGF) or Bridgman, the Czochralski method, and solidification on a seed with no crystal pulling and no crystal rotation. In all growth methods, the time of holding the starting material in the liquid phase was no longer than 5 h (depending on the starting composition). A long growth time (e.g., 20 h) leads to a high composition shift and ceramic formation instead of a single crystal. Cooling time from the solidification point to room
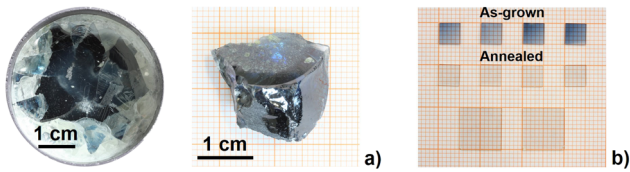
FIG. 2. Undoped bulk $ZnGa_2O_4$ single crystals obtained from the melt by the VGF/Bridgman method (a), and (100)-oriented wafers prepared from the as-grown and annealed bulk crystals (b).

temperature was 8–12 h. Alternative techniques suitable for melt growth of $ZnGa_2O_4$ are shaped growth methods utilizing shapers (e.g., Edge-Defined Film-Fed Growth, EFG) that typically apply relatively high growth rates. For all melt growth methods, it is important to minimize the composition shift by combining non-stoichiometric starting composition (ZnO excess), relatively short growth time, high oxygen partial pressure, preferably an overpressure (≫1 bar), and low temperature gradients above the melt surface to minimize incongruent evaporation.

In proper growth conditions, the ZnO-Ga_2O_3 system solidifies from the melt in the single crystalline phase of $ZnGa_2O_4$ with clear blue coloration [Fig. 2(a)], which may vary from colourless through light blue and blue to dark blue depending on growth conditions. Typically, the crystal coloration becomes lighter with increasing ZnO excess in the starting composition, oxygen concentration in the growth atmosphere, and overpressure. The blue coloration is associated with the free carrier absorption in the near infrared and the red part of the visible spectral regions (see Fig. 14). The crystals become darker with the free carrier concentration. The crystallized material within a crucible typically consists of a few large single crystals with a volume up to about 3 cm^3 each. From such large single crystals, wafers of high structural quality and size of 5×5 and 10×10 mm^2 could be easily fabricated [Fig. 2(b)]. The wafer fabrication is quite easy as it is cubic with no preferred cleavage planes.

Thermal stability of the obtained crystals is important from the point of view of epitaxial growth, when the crystals are used as substrates, and for high temperature device operation, e.g., as gas sensors. A number of crystal samples were annealed in an oxidizing atmosphere (air) at temperatures 500–1400 °C for 10, 20, or 40 h and in a reducing atmosphere (5% H_2 + 95% Ar) at 300–800 °C for 10 h. Additionally, some of the $ZnGa_2O_4$ samples were annealed at the same conditions but were embedded either in a ZnO or Ga_2O_3 powder. Mass change of the samples after annealing is shown in Fig. 3. After annealing in air, the crystals are stable up to about 1100 °C with 10 h annealing time. At this temperature, a small decomposition proceeds, which enhances with temperature, reaching a mass loss of about 2.3 wt. % after 10 h annealing at 1400 °C. When the samples were embedded in Ga_2O_3 powder, the mass loss was comparable or a bit larger as compared to the samples exposed directly to air. Surprisingly, samples embedded in ZnO powder showed a significant gain in mass, which increased with annealing temperature. After annealing at 1200 and 1400 °C, the mass gain was as high as 0.47 and 36 wt. %, respectively. A close inspection of the sample surfaces revealed a precipitation of ZnO crystal fibres from the ZnO powder, as shown in Fig. 4. Upon annealing in the reducing atmosphere, $ZnGa_2O_4$ crystal samples were substantially stable up to about 700 °C, above which a very strong decomposition proceeds. After annealing at 800 °C for 10 h, the mass loss reached the value of 11 wt. %. Here embedding the crystal samples in ZnO and Ga_2O_3 powders prevented decomposition of the crystal samples up to 750 °C, as no mass loss or gain was measured.

Thermal analysis (DTA/TG) of crystal samples from different growth experiments exhibited an exothermic peak at 720–730 °C upon heating up at 20 K/min (the same effect was observed at heating-up rate of 10 and 5 K/min), which may indicate atom re-arrangement within the crystal lattice. A similar effect we observed for $MgGa_2O_4$.[51] Exothermal effects during heating curves are untypical and give a hint that the samples are in a metastable non-equilibrium state that changes upon heating to equilibrium under the release of energy. To reveal this, other long-term measurements were performed with one piece of a $ZnGa_2O_4$ single crystal, using a DSC (differential scanning calorimetry) sample carrier instead of the DTA carrier.

The idea behind these measurements is as follows: in general, spinels are represented by the chemical formula
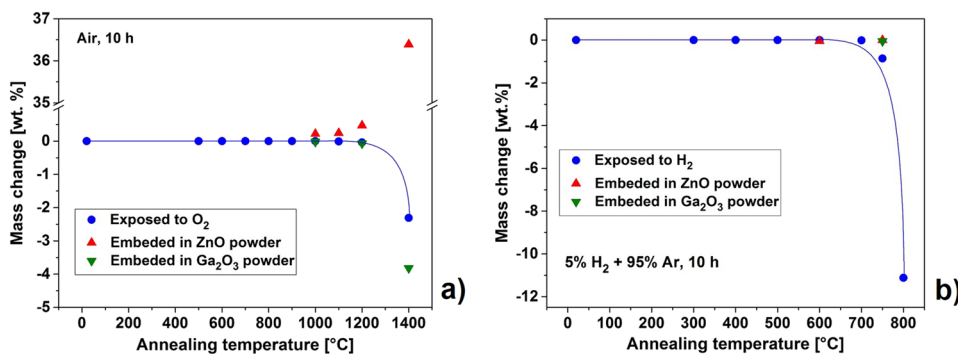

FIG. 3. Mass change of $ZnGa_2O_4$ crystal samples after annealing in oxidizing (a) and reducing conditions (b).

FIG. 4. ZnO overgrowth on a $ZnGa_2O_4$ wafer embedded in ZnO powder during annealing in air at 1200 °C for 10 h with the mass gain of 0.47 wt. %.

$A_{1-x}B_x(A_xB_{2-x})O_4$, where x is the degree of inversion that spans between 0 ("normal spinel") and 1 ("inverse spinel"), where B-atoms (here Ga) occupy all tetrahedral sites. According to O'Neill and Navrotsky,[52] $ZnGa_2O_4$ is a normal spinel ($x \approx 0$). It is a specific feature of spinel compounds that at high temperatures A and B atoms are more and more statistically distributed across lattice sites, approaching a random distribution with $x \approx 2/3$. This random distribution with larger disorder has a configurational entropy that is larger than for $x = 0$ by $S_c \approx 15.88$ J/mol^{-1} K^{-1}. A structure with higher entropy is expected to have a higher specific heat capacity because c_p is the integral over S/T (T–temperature).

Figure 5 shows five DSC curves that were obtained from the same $ZnGa_2O_4$ crystal sample during heating runs (20 K/min) after equilibrating the material for different periods of times at 600 °C. This is substantially below the exothermal DTA peaks mentioned above, where equilibration occurs spontaneously under the release of heat. The uppermost curve
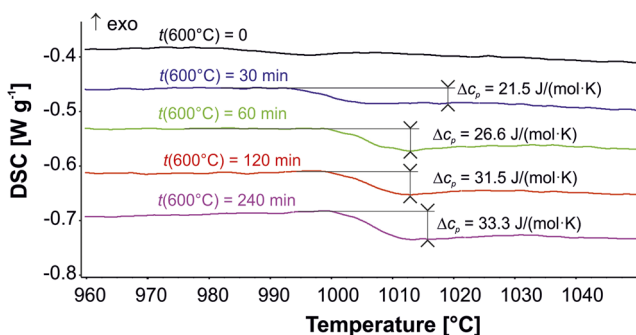
in Fig. 5 was obtained immediately after cooling the sample quickly from 1200 °C (more random distribution) to 600 °C (more normal distribution). No significant thermal effects are visible during heating. The lower curves were obtained after annealing the sample for the designation periods of time (30–240 min) at 600 °C. One sees that a shift toward an endothermal reaction occurs near 1000 °C, and the amplitude of this shift rises with the holding time at 600 °C. It should be noted that an endothermal shift of the DSC curve indicates a higher c_p value. It is obvious that a sufficient annealing time around 2 h is required to approach equilibrium cation distribution at 600 °C.

Although $ZnGa_2O_4$ is a normal spinel, at high temperatures during growth from the melt, Zn^{2+} and Ga^{3+} ions are distributed randomly at tetrahedral and octahedral sites in the spinel structure, as mentioned above. During cooling down, Zn^{2+} and Ga^{3+} tend to occupy tetrahedral and octahedral sites, respectively. If the cooling time is not long enough, the obtained crystals may not be a fully normal spinel, but partly random, as not all ions have occupied own designated positions. Such arrangement changes the electronic structure of $ZnGa_2O_4$ and may lead, likely indirectly, to electrical conductivity. Annealing above 700 °C for at least 10 h in the presence of oxygen leads to a complete re-arrangement of Zn^{2+} and Ga^{3+} ions to form normal spinel. As the result of annealing, the blue crystals became colourless.

An additional feature on possible structural changes above 700 °C can be recognised from the thermal conductivity vs. temperature shown in Fig. 6. Around 700–750 °C, there is a well distinguished step-like formation that can be related to the change of cation occupancy site contributing to the heat transport. Such anomaly in thermal transport was also measured in the case of $MgGa_2O_4$ around 1050 °C.[53] At room temperature, the thermal conductivity of $ZnGa_2O_4$ is

FIG. 5. Five subsequent heating segments (20 K/min) of 41.32 mg $ZnGa_2O_4$ single crystal. Prior reaching each of the heating curve, the sample was hold for 60 min at 1200 °C and cooled-down with 30 K/min to 600 °C. The parameter t(600 °C) at each curves refers to the holding time at 600 °C.
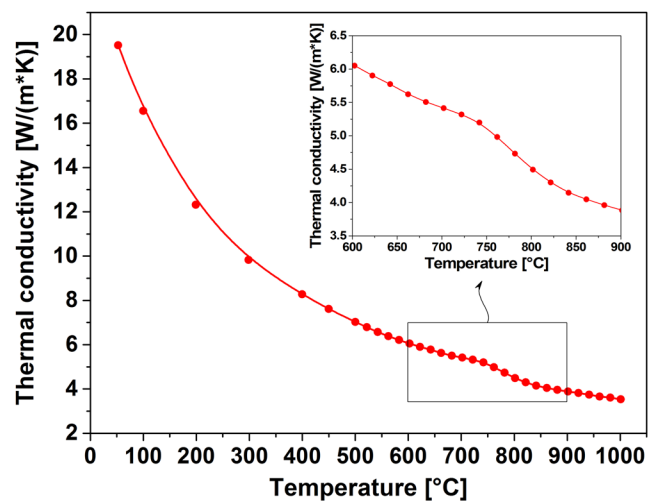

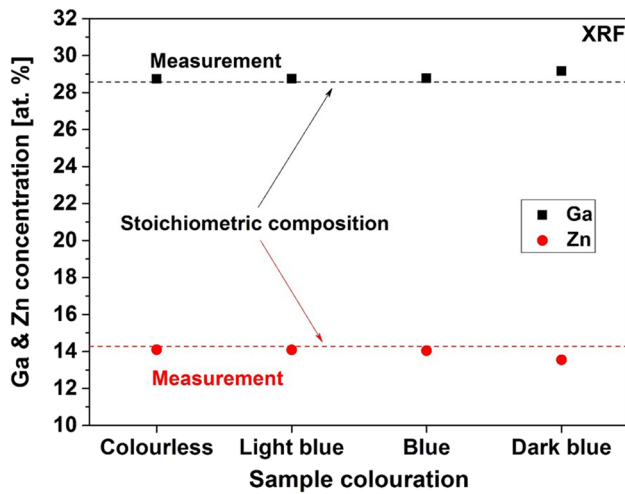FIG. 6. Thermal conductivity of $ZnGa_2O_4$ single crystal vs. temperature.

FIG. 7. Ga and Zn concentrations measured by XRF in various ZnGa$_2$O$_4$ crystals having different colourations. The experimental error within is within the size of the circle and square symbols.
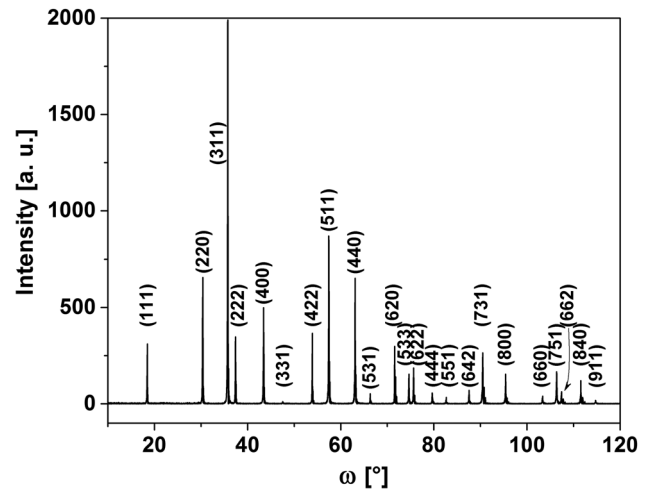

FIG. 8. XRD pattern of powdered ZnGa$_2$O$_4$ single crystals with stoichiometric or near-stoichiometric composition.

22.1 W m^{-1} K^{-1}, comparable to that of β-Ga$_2$O$_3$ along [001] axis (21 W m^{-1} K^{-1}).[54]

Figure 7 shows Ga and Zn concentrations in various ZnGa$_2$O$_4$ crystal samples having different colourations, which were determined by XRF. The colourless samples have stoichiometric or almost stoichiometric composition. A characteristic feature is an increased deviation from stoichiometry toward Ga excess with darker crystal colouration, which is visible in both methods, i.e., the crystal stoichiometry deviation increases with the following coloration order: colourless → light blue → blue → dark blue. The same compositional trend vs. crystal colouration was observed in the case of measuring the Ga and Zn concentrations by using the ICP-OES method. Annealing the crystals in the presence of oxygen at or above 800 °C for 10 h or longer turns the blue crystals into colourless ones. Removal of the colouration could be achieved also at 700 °C but at long annealing time of at least 40 h. Annealing of ZnGa$_2$O$_4$ crystals in the presence of oxygen at temperatures below 700 °C had substantially no impact on the crystal colouration. Interestingly, annealing in the presence of hydrogen for 10 h did not change the crystal colouration after annealing up to 700 °C. The crystals annealed at 800 °C became only a bit darker and still remained fully transparent. A bit darker colouration appeared after annealing of ZnGa$_2$O$_4$ crystals embedded in ZnO powder at 600 °C for 10 h in the presence of hydrogen; however, annealing at the same conditions but in the presence of oxygen did not affect the crystal colouration.

The crystals obtained from the melt at high oxygen concentrations (≥20 vol.%) and external overpressure (2 or 10 bars) or with the ZnO excess in the starting material and at atmospheric pressure produced crystals were substantially colourless or a bit yellowish at the top part of the crucible that

had a direct contact with the growth atmosphere, and blue underneath. With lower oxygen concentration, the crystals at the top part of the crucible are light blue, which become dark in a deeper part of the crucible.

The ω-scan of XRD of powdered crystals is shown in Fig. 8. According to the PDF 28-1240 file, the obtained phase is a pure ZnGa$_2$O$_4$ spinel with no other phases within the accuracy of the XRD. This is just a confirmation of composition analysis that proves stoichiometric or near-stoichiometric composition of ZnGa$_2$O$_4$ crystals grown from the melt. Such a pattern was obtained for all single crystalline samples with different colourations, from colourless to dark blue.
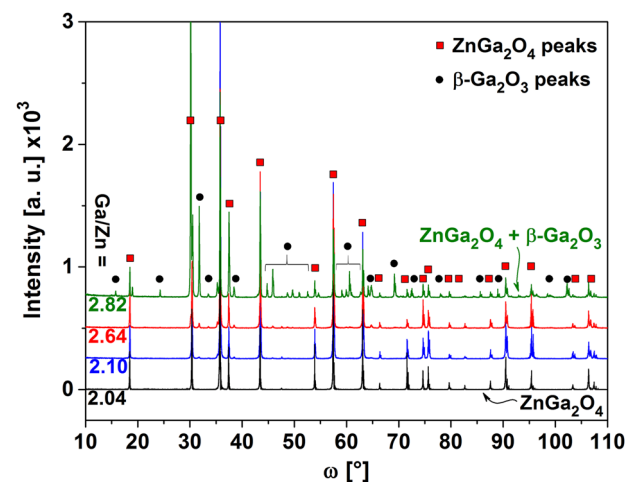

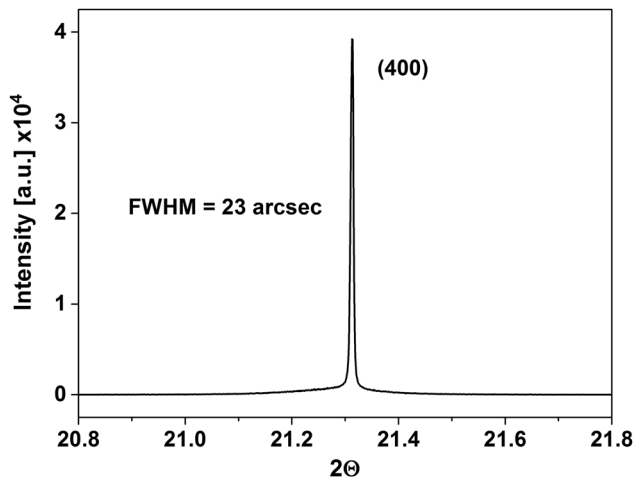**FIG. 9**. XRD patterns of powdered ZnGa$_2$O$_4$ single crystals with different compositions.

FIG. 10. Rocking curve of one of the (100)-oriented $ZnGa_2O_4$ wafer shown in Fig. 2(b).

shown in Fig. 10. Single peak of the rocking curve indicates one single orientation without low-angle grain boundaries.

Etching of polished $ZnGa_2O_4$ wafers in NaOH at 100 °C for 1 h lead to the formation of crystallographically oriented, arrow-like pits at the surface of the samples with a density of about $\sim 10^7$ cm^{-2} [Fig. 11(a)]. $ZnGa_2O_4$ is resistant to aqueous solutions of H_3PO_4 and HCl, as hot etching in such solutions did not reveal any pits. On the other hand, dry etching of the polished wafers in air at 1400 °C for 10 h showed crystallographically oriented structure consisting of squares, rectangles, and perfect pyramids with a square base, as depicted in Fig. 11(b).

Figure 12(a) shows a high-resolution transmission electron microscopic (HRTEM) image of the $ZnGa_2O_4$ lattice along the ⟨100⟩ direction under NCSI [negative spherical aberration (CS) imaging] conditions,[55] i.e., atoms appear as bright spots. The image is superimposed by a multislice simulation of the HRTEM image for a sample thickness of 6 nm and a defocus of −12 nm. For a better comparison, also a stick and ball model of the structure is shown in Fig. 12(b). Under these conditions, the highest intensity spots in the image are located between the atomic columns, while the slightly darker columns correspond to Zn columns. Green, gray, and red balls correspond to Ga, Zn, and O columns, respectively. TEM bright field investigations of an as-grown and colourless crystal sample (Fig. 13) revealed the presence of small, crystallographically oriented particles inside the $ZnGa_2O_4$ matrix. From the formation of the Moiré pattern at the particles, we can conclude that these particles are crystalline species having a different lattice parameter or crystallographic orientation with respect to the matrix. The nature of these particles is still under investigation, but one may hypothesize that it is either metallic Ga or Ga_2O_3 that forms through a deficiency of Zn. The density of these particles is in the range of 5×10^{14} cm^{-3}.

Nominally undoped $ZnGa_2O_4$ crystals were examined by conductivity and Hall effect measurements in the as-grown state and after post-growth heat treatments. Undoped, as-grown crystals of light blue, blue, and dark blue coloration (see Table I) were n-type semiconductors which are characterized by resistivities of 0.002–0.1 Ωcm, electron concentrations of 3×10^{18}–9×10^{19} cm^{-3}, and electron mobilities of about 40–100 cm^2 V^{-1} s^{-1}. It is worth to mention that the

However, longer times (>5 h at atmospheric pressure) of keeping $ZnGa_2O_4$ in the liquid phase leads to a significant compositional change that produces another phase. The XRD ω-scans of molten $ZnGa_2O_4$ samples with different deviations from stoichiometry, defined as the Ga/Zn atomic ratio, are collected in Fig. 9. Too high losses of Zn lead to an excess of Ga that causes the formation of the β-Ga_2O_3 phase in addition to the $ZnGa_2O_4$ phase. According to the XRD patterns, the β-Ga_2O_3 phase occurred at Ga/Zn = 2.64 and 2.82. The material with $2 \leq$ Ga/Zn ≤ 2.17 was still a single crystal, while with Ga/Zn ≥ 2.8–a yellow ceramic. The spinel structure enables some deviation from stoichiometry while keeping single crystalline form. The Ga/Zn ratio is preserved after annealing in the presence of oxygen up to 1100 °C for 10 h. The lattice parameter that we measured on an as-grown colourless sample yielded a value of 8.3336 ± 0.0019 Å.

Rocking curve measurements on (100)-oriented $ZnGa_2O_4$ crystal samples of Fig. 2(b) by HR XRD revealed a very good structural quality of the obtained crystals. The full width at half maximum (FWHM) of the rocking curve of the 400 peak on the (100) face was typically below 50 arcsec, such as 23 arcsec
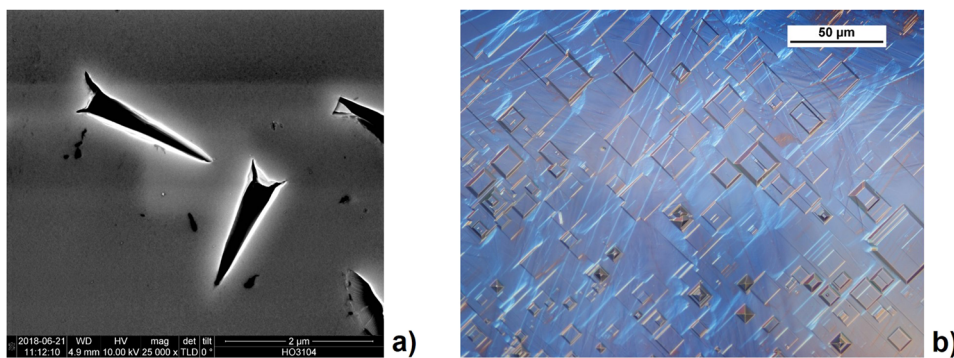

FIG. 11. Etch pits revealed in $ZnGa_2O_4$ wafers by wet etching in NaOH at 100 °C for 1 h (a) and dry etching in air at 1400 °C for 10 h (b).
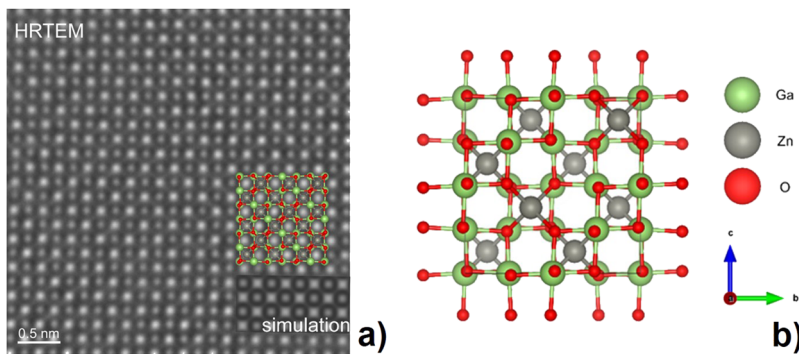
FIG. 12. HRTEM image of an as-grown and colourless $ZnGa_2O_4$ crystal sample along $\langle 100 \rangle$ direction (a) and stick and ball model (b).

highest electron mobility of about 100 cm^2 V^{-1} s^{-1} was measured at high electron concentrations of 1–2×10^{19} cm^{-3}. The measured electron mobilities are in the range of other TCOs and compatible with the theoretically predicted electron effective mass, by Karazhanov and Ravindran,[56] Dixit *et al.*,[57] Sampath *et al.*,[58] of about 0.22–$44m_0$ (m_0 is the free electron mass).

Only high values of the free electron concentration ($>10^{18}$ cm^{-3}) that were conducted from the Hall effect measurements may lead to a conclusion of the presence of a mechanism blocking the current flow at low values of the free electron concentration.

This could be the presence of particles with the Moiré pattern shown in Fig. 13. These precipitates may introduce interface states between themselves and the surrounding $ZnGa_2O_4$ matrix. These interface states may act as deep compensating centres. Hence, this may have the same effect like the incoherent twin boundaries in β-Ga_2O_3 (100) films that create dangling bonds acting as Schottky barriers for the current flow basing on the model developed by Fiedler *et al.*[59] and Schewski *et al.*[60] We conclude that the density of the particles in $ZnGa_2O_4$ crystals at the level of mid 10^{14} cm^{-3} (mean distance between each particle is $\approx$120 nm) is sufficient to block the current flow at free electron concentration levels below

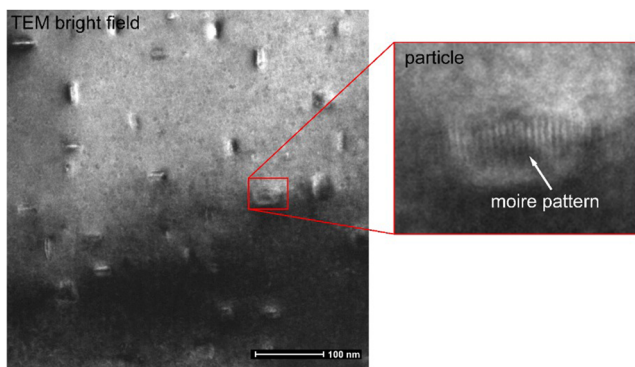10^{18} cm^{-3} (charge depletion width $\approx$30 nm). With such a charge depletion region around each precipitate, half of the crystal is depleted, which is detrimental for the charge transport. The nature and elimination of these particles may lead to lower and well controllable levels of the free electron concentrations with the Hall mobility well exceeding 100 cm^2 V^{-1} s^{-1}, similar to β-Ga_2O_3 (100) films.

Annealing of as-grown $ZnGa_2O_4$ crystals in the oxidizing atmosphere (air or O_2) at 800–1400 °C for 10 h resulted in colourless and electrically insulating crystals independent on their original conductivity and coloration. The same effect could be obtained at 700 °C, but the annealing time must be longer, 40 h or more. Annealing at temperatures <700 °C has substantially no impact on the electrical conductivity. It is remarkable that the discontinuity in the thermal conductivity vs. temperature behavior (Fig. 6) as well as the exothermal DTA peak was observed in this same T-range were annealing becomes effective–probably here the mobility of atoms becomes significant.

Annealing of as-grown (blue) $ZnGa_2O_4$ in the presence of H_2 at 300–800 °C for 10 h basically does not affect the crystal coloration; they are getting only a bit darker after annealing at 700 °C–800 °C, which is partly associated with some decomposition. Annealing of colourless and electrically insulating crystals in the presence of hydrogen turned the crystals into a semiconducting state when annealed at or above 700 °C for about 10 h or longer. The electron concentration was 2–3×10^{18} cm^{-3}, while the electron mobility was about 20 cm^2 V^{-1} s^{-1}, lower as compared to that of as-grown crystals.

$ZnGa_2O_4$ crystals annealed in air while embedded in the Ga_2O_3 powder behave electrically in the same way as the crystal exposed directly to air, i.e., they became fully colourless and electrical insulators, when annealed at temperatures above 800 °C (or at 700-800 °C for extended annealing time $\geq$40 h). Also $ZnGa_2O_4$ crystals annealed in air while embedded in the ZnO powder were electrical insulators when annealed at temperatures 800–1200 °C.

Annealing of $ZnGa_2O_4$ crystals in the presence of hydrogen while embedded in Ga_2O_3 and ZnO powders substantially did not affect the electrical properties as compared to

FIG. 13. TEM bright field image of an as-grown and colourless $ZnGa_2O_4$ single crystal revealing particles with a Moiré pattern.

TABLE I. Electrical properties of as-grown and annealed bulk $ZnGa_2O_4$ single crystals having different colorations. n, μ, and ρ are the free electron concentration, Hall mobility, and resistivity, respectively.

Sample	n (cm^{-3})	μ [cm^{2}V^{-1}s^{-1}]	ρ (Ωcm)
As-grown (colourless, yellowish)		Electrical insulator	
As-grown (light-blue)	3–6×10^{18}	20–30	0.1–0.04
As-grown (blue)	6×10^{18}–1×10^{19}	45–80	~0.01
As-grown (dark blue)	1–9×10^{19}	40–100	0.002–0.004
Annealed: air, ≥ 700 °C, ≥ 10 h (colourless)		Electrical insulator	
Annealed: H$_2$, 300–800 °C, 10 h (blue)	6×10^{18}–3×10^{19}	40–107	0.02–0.002

those of as-grown crystals, when annealed at temperatures up to 750 °C. Higher annealing temperatures lead to a strong decomposition and surface deterioration.

The $ZnGa_2O_4$ crystals doped with Si^{4+} and Zr^{4+} (about 0.2 mol. %) showed substantially the same electrical properties as undoped crystals. The potential contribution of the dopants to the electrical conductivity was likely overlapped by the "intrinsic" conductivity (here "intrinsic" means only with no intentional doping). It is rather difficult to conclude which of the Zn^{2+} or Ga^{3+} sites are substituted by the Si^{4+} and Zr^{4+} dopants, as both ions occupy both octahedral and tetrahedral sites in the spinel structure.

Whether the underlying donors are native defects, impurities, or a mixture of both is presently unclear. One should note that even for much more detailed investigated transparent semiconducting oxides the origin of conductivity is still controversially discussed. Therefore, we avoid any speculations in this respect until future studies (including e.g., defect spectroscopy) bring a clear picture in this matter.

The optical transmittance in the spectral range from 180 nm to 2500 nm is shown in Fig. 14 for a blue (as-grown, black spectrum in Fig. 14) and 2 colourless (annealed in air, 800 °C, 10 h, blue and red lines in Fig. 14) samples, respectively [see Fig. 2(b)]. The blue sample was semiconducting with the free electron concentration of about 10^{19} cm^{-3}, while the colourless samples were electrical insulators. All samples exhibit a sharp absorption edge at about 275 nm. The semiconducting sample shows a strong absorption in the red and near infrared region due to free carrier absorption, and the colourless samples are fully transparent in the whole measured spectrum. Interestingly, all as-grown and annealed (in both O$_2$ and H$_2$−containing atmospheres) samples reveal a weak absorption around 325 nm. One explanation would be the absorption by surface plasmons at metallic particles, as proved in the case of In$_2$O$_3$.[61] As shown in Fig. 9, we observed particles embedded in the $ZnGa_2O_4$ host lattice.

The transmittance of the colourless samples increases remarkable from 80.65% to 82.52% between 1000 nm and 2000 nm. Assuming negligible losses due to scattering by using integrating sphere detection, the measured transmittance T in this non-absorbent wavelength range is only reduced by the reflectance R of the two sample surfaces. For normal incidence

of light, the relation T = (1 − R)/(1 + R) ≈ $2n/(n^2 + 1)$[49] can be used to determine the refractive index n. Using this assumption, we estimate for $ZnGa_2O_4$ a refractive index $n = 1.97 \pm 0.01$ for the wavelength of 1000 nm, which decreases to 1.90 at 2000 nm.

Theoretically, the bandgap of $ZnGa_2O_4$ was predicted to be indirect (K–Γ) with a value of 2.69 eV,[62] 2.7 eV,[63] 2.78 eV,[64] 2.8 eV,[56] 4 eV,[48] 4.57–4.71 eV,[57] and 4.39 eV,[65] or direct (Γ–Γ) with the bandgap of 2.79 eV.[58] The experimental bandgap was found at the values of 4.1–4.3 eV measured on synthetized ZnO:Ga$_2$O$_3$ powders,[66] about 5 eV on ceramics,[45] 5 (direct) and 4.6 (indirect) eV measured on films obtained by mist-CVD,[39] about 4.9 eV on films obtained by sol-gel,[23] and 4 eV on bulk crystals obtained by the flux method.[43] Theoretical discrepancy in energy gap values arises from computational methods, while experimental ones arise from a stoichiometry deviation.

Having substantially stoichiometric bulk single crystals of high structural quality as compared to previously measured samples, we could estimate the optical bandgap of $ZnGa_2O_4$ more accurately. Plotting the absorption coefficient for direct and indirect transitions, we concluded a much better linear fit
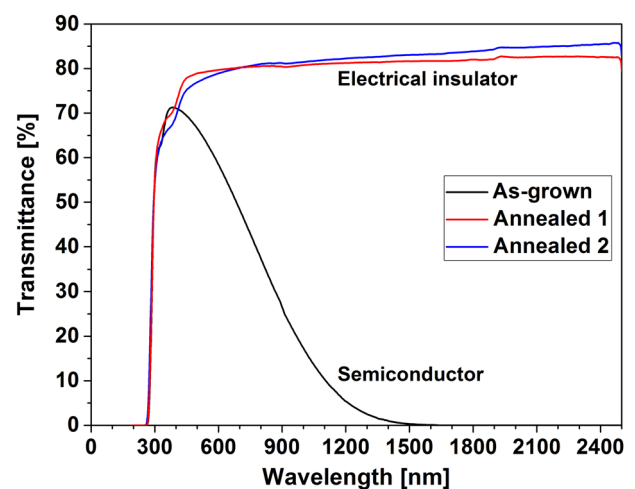
FIG. 14. Optical transmittance spectra of as-grown (black line) and air-annealed (blue and red lines) $ZnGa_2O_4$ crystal samples.
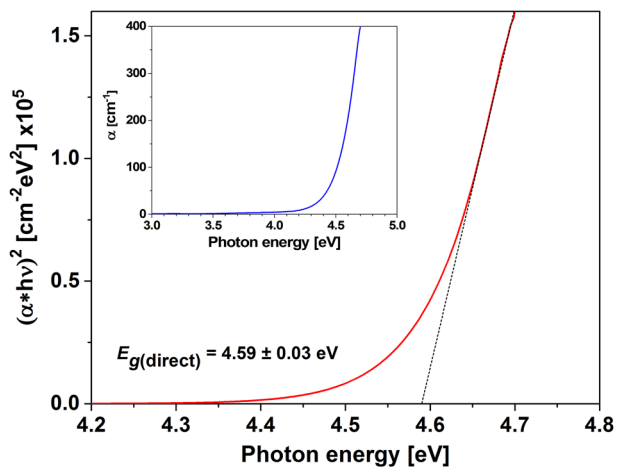
FIG. 15. Absorption coefficient α in power 2 versus photon energy that corresponds to direct transitions. Dashed black line indicates an extrapolation of the linear part of the curve. The inset shows a spectral dependence of the absorption coefficient measured for the colourless transparent sample having a thickness of 250 μm.

to the direct transition, as shown in Fig. 15, with the absorption coefficient in the inset. The estimated bandgap for the direct transition is 4.59 ± 0.03 eV, while for the indirect transition, it is about 4.33 eV.

To better understand potentials of $ZnGa_2O_4$ for electronic and optoelectronic applications, we compare basic features of bulk crystals of this compound with our bulk β-Ga_2O_3 single crystals obtained by the Czochralski method,[50,67,68] as summarized in Table II. An important point is the possibility of growing $ZnGa_2O_4$ crystals directly from the melt, the same as β-Ga_2O_3. It is thermally more unstable than β-Ga_2O_3 due to much higher $p(Zn)$ than $p(Ga_2O)$ leading to a incongruent evaporation, and higher melting point by about 100 K, but large volumes could be grown by the VGF, seeded solidification, and the Czochralski methods. Although the volume of $ZnGa_2O_4$ single crystals from one growth experiment is about 8 cm^3, much smaller than that of Ga_2O_3 obtained by the Czochralski method (about 160 cm^3), it is just a demonstration with further scale-up capabilities. An advantage of $ZnGa_2O_4$ is a cubic system with no distinguished cleavage planes. This enables an easier growth of large volume crystals and easier wafer fabrication. Moreover, cubic systems are better fitted substrates for epitaxial growth, than the monoclinic β-Ga_2O_3. The fundamental bandgap of $ZnGa_2O_4$ is similar to that of β-Ga_2O_3 with the polarization parallel to the [001] and [100] axes. This feature enables to use $ZnGa_2O_4$ in UV optoelectronics and high power electronics, the same as β-Ga_2O_3. The thermal conductivity of Ga_2O_3 is highly anisotropic with the values of 13, 21, and 29 W m^{-1} K^{-1} along [100] [001], and [010] axes, respectively,[54] while that of $ZnGa_2O_4$ is isotropic with the value of about 22 W m^{-1} K^{-1} at room temperature, similar to that of the β-Ga_2O_3 along [001] axis. $ZnGa_2O_4$ may have a very high electrical conductivity without intentional doping, higher than β-Ga_2O_3 even by one order of magnitude. Also the electron mobility of $ZnGa_2O_4$ at very high electron concentration was measured twice higher than in β-Ga_2O_3. Both materials can be obtained as electrical insulators. It seems, however, it is more difficult to obtain lower level of the free electron concentrations ($<10^{18}$ cm^{-3}) in $ZnGa_2O_4$, which is not an intrinsic property, but rather the result of the presence of nanoparticles in the host (see Fig. 13). Nonetheless, further study of the material properties combined with growth conditions for bulk crystals and homoepitaxial film growth with controlled doping concentrations may boost the development

TABLE II. Basic features of bulk single crystals of β-Ga_2O_3 and $ZnGa_2O_4$ grown from the melt.

	β-Ga_2O_3	$ZnGa_2O_4$
Status	Advanced development	First experiments
Melt growth method	Czochralski	VGF, Czochralski
Melting point (°C)	~1800	~1900
Max. volume of a single crystal in one run (cm^3)	160	8
Crystal system	Monoclinic	Cubic
Easy cleavage planes	{100} and {001}	None
Wafer fabrication (slicing, polishing)	Difficult	Easy
Energy gap (eV)	4.56 ‖ [001] direct 4.59 ‖ [100] direct 4.85 ‖ [010] direct	4.570 direct 4.325 indirect
Basic electrical properties of undoped crystals	$n = 5 \times 10^{16}$–2×10^{18} cm^{-3} $\mu = 100$–150 cm^2 V^{-1} s^{-1} $\rho = 1$–0.04 Ωcm	$n = 3 \times 10^{18}$–9×10^{19} cm^{-3} $\mu = 40$–100 cm^2 V^{-1} s^{-1} $\rho = 0.1$–0.002 Ωcm
Max. electron concentration (cm^{-3})	10^{19} (by doping with Si or Sn)	~10^{20} (unintentionally doped)
Max. mobility at high electron concentration ($\geq 10^{19}$ cm^{-3}) (cm^2 V^{-1} s^{-1})	50	107
Electrical insulator possible?	Yes	Yes
Thermal conductivity at room temperature [W m^{-1} K^{-1}]	Along [100] = 11 Along [010] = 29 Along [001] = 21	22.1

TABLE III. Lattice constants of various Fe-based spinels and $ZnGa_2O_4$ spinel along with lattice mismatch inbetween. Lattice mismatch is calculated from the formula $(a_{layer} - a_{substrate})/a_{substrate}$.

Material	$ZnGa_2O_4$	NiF_2O_4	$CoFe_2O_4$	$ZnFe_2O_4$	$MnFe_2O_4$
Lattice constant (Å)	8.3336	8.337	8.392	8.441	8.449
Lattice mismatch with $ZnGa_2O_4$ (%)	–	0.04	0.74	1.33	1.43

of $ZnGa_2O_4$ to a similar technological level as in the case of bulk β-Ga_2O_3 crystals.

In addition to potential applications in electronics and UV optoelectronics, bulk $ZnGa_2O_4$ single crystals can serve as substrates for epitaxial growth of some of magnetic materials, such as ferrites having spinel structures. Commonly used $MgAl_2O_4$ (a = 8.086 Å) substrates generate large lattice mismatch with ferrite spinels (e.g., 3.1% with $NiFe_2O_4$), and lead to anti-phase boundaries. It has been shown, however, that our Ga-based spinels $MgGa_2O_4$ (a = 8.280 Å) and $CoGa_2O_4$ (a = 8.328 Å) eliminated anti-phase boundaries in nickel ferrite ($NiFe_2O_4$) thin films[69] due to low lattice mismatch between the substrates and films grown thereon, 0.69% and 0.11%, respectively. $ZnGa_2O_4$ has even better lattice match to $NiFe_2O_4$ (0.04%). This also applies to other ferrite spinels, such as $CoFe_2O_4$, $ZnFe_2O_4$, $MnFe_2O_4$, and $MgFe_2O_4$ that have lattice mismatch with $ZnGa_2O_4$ below 1.5% and may substitute commonly used $MgAl_2O_4$ spinel as the substrate. Availability of bulk $ZnGa_2O_4$ crystals may bring the development of magnetic films to a higher level in terms of the structural quality and magnetic properties of the films. Lattice parameters of selected ferrite spinels together with $ZnGa_2O_4$ are shown in Table III.

We demonstrated the growth and characterization of truly bulk $ZnGa_2O_4$ single crystals obtained directly from the melt. A high melting point of $ZnGa_2O_4$ of 1900 ± 20 °C leads to its thermal decomposition in the liquid phase and to intensive incongruent evaporation resulted in a composition shift. Optimized growth conditions resulted in stoichiometric or near-stoichiometric single crystals with a normal spinel structure. $ZnGa_2O_4$ maintains a single crystalline structure with the Ga/Zn ratio up to about 2.17, above which an admixture of β-Ga_2O_3 is formed. The obtained single crystals were of good structural quality characterized by the FWHM of the rocking curve of (100)-oriented wafers even below 25 arcsec. $ZnGa_2O_4$ single crystals could be either electrical insulators or n-type semiconductors with the resistivity, free electron concentration, and Hall mobility of 0.002–0.1 Ωcm, 3×10^{18}–9×10^{19} cm^{-3}, and 40–107 cm^2 V^{-1} s^{-1}, respectively. The semiconducting state could be switched into electrically insulating state by annealing in the presence of oxygen at temperatures ≥700 °C for at least several hours. Transmittance spectra show a steep absorption edge at 275 nm, while the optical bandgap concluded from the absorption coefficient is direct with a value of about 4.6 eV. Melt-grown $ZnGa_2O_4$ single crystals are thermally stable up to 1100 and 700 °C upon annealing in oxidizing and reducing atmospheres, respectively. Being cubic and having no easy cleavage planes,

$ZnGa_2O_4$ crystals enable easy wafer fabrication not only for electronic and optoelectronic applications but also can serve as good lattice matched substrates for epitaxial growth of magnetic ferrite spinel films.

REFERENCES

[1]M. Grundmann, H. Frenzel, A. Lajn, M. Lorenz, F. Schein, and H. von Wenckstern, Phys. Status Solidi A **207**, 1437–1449 (2010).

[2]M. Lorenz, M. S. R. Rao, T. Venkatesan, E. Fortunato, P. Barquinha, R. Branquinho, D. Salgueiro, R. Martins, E. Carlos, A. Liu, F. K. Shan, M. Grundmann, H. Boschker, J. Mukherjee, M. Priyadarshini, N. D. Gupta, D. J. Rogers, F. H. Teherani, E. V. Sandana, P. Bove, K. Rietwyk, A. Zaban, A. Veziridis, A. Weidenkaff, M. Muralidhar, M. Murakami, S. Abel, J. Fompeyrine, J. Zuniga-Perez, R. Ramesh, N. A. Spaldin, S. Ostanin, V. Borisov, I. Mertig, V. Lazenka, G. Srinivasan, W. Prellier, M. Uchida, M. Kawasaki, R. Pentcheva, P. Gegenwart, F. M. Granozio, J. Fontcuberta, and N. Pryds, J. Phys. D: Appl. Phys. **49**, 433001 (2016).

[3]E. Fortunato, P. Barquinha, and R. Martins, Adv. Mater. **24**, 2945–2986 (2012).

[4]S. J. Pearton, J. Yang, P. H. Cary IV, F. Ren, J. Kim, M. J. Tadjer, and M. A. Mastro, Appl. Phys. Rev. **5**, 011301 (2018).

[5]M. Higashiwaki, H. Murakami, Y. Kumagai, and A. Kuramata, Jpn. J. Appl. Phys., Part 2 **55**, 1202A1 (2016).

[6]K. Irmscher, M. Naumann, M. Pietsch, Z. Galazka, R. Uecker, T. Schulz, R. Schewski, M. Albrecht, and R. Fornari, Phys. Status Solidi A **211**, 54–58 (2014).

[7]C. Janowitz, V. Scherer, M. Mohamed, A. Krapf, H. Dwelk, R. Manzke, Z. Galazka, R. Uecker, K. Irmscher, R. Fornari, M. Michling, D. Schmeißer, J. R. Weber, J. B. Varley, and C. G. Van de Walle, New J. Phys. **13**, 085014 (2011).

[8]M. G. Brik, A. Suchocki, and A. Kamińska, Inorg. Chem. **53**, 5088–5099 (2014).

[9]S. Itoh, H. Taki, Y. Sato, K. Morimoto, and T. Kishino, J. Electrochem. Soc. **138**, 1509–1512 (1991).

[10]T. Minami, T. Maeno, Y. Kuroi, and S. Takata, Jpn. J. Appl. Phys., Part 2 **34**, L684–L687 (1995).

[11]P. D. Rack, J. J. Peterson, M. D. Potter, and W. Park, J. Mater. Res. **16**, 1429–1433 (2001).

[12]A. Bessière, S. Jacquart, K. Priolkar, A. Lecointre, B. Viana, and D. Gourier, Opt. Express **19**, 10131–10137 (2011).

[13]J. S. Kim, J. S. Kim, T. W. Kim, H. L. Park, Y. G. Kim, S. K. Chang, and S. D. Han, Solid State Commun. **131**, 493–497 (2004).

[14]E. Rusu, V. Ursaki, G. Novitschi, M. Vasile, P. Petrenco, and L. Kulyuk, Phys. Status Solidi C **6**, 1199–1202 (2009).

[15]J. S. Kim, H. L. Park, G. C. Kim, T. W. Kim, Y. H. Hwang, H. K. Kim, S. I. Mho, and S. D. Han, Solid State Commun. **126**, 515–518 (2003).

[16]G. Anoop, K. M. Krishna, and M. K Jayaraj, J. Electrochem. Soc. **158**, J269–J272 (2011).

[17]Z. Lou, L. Li, and G. Shen, Nano Res. **8**, 2162–2169 (2015).

[18]X. Li, X. Zhang, X. Zheng, Y. Shao, M. He, P. Wang, X. Fu, and D. Li, J. Mater. Chem. A **2**, 15796 (2014).

[19]C. Chen, G. Li, and Y. Liu, Powder Technol. **281**, 7–11 (2015).

[20]L.-C. Cheng, C.-Y. Huang, and R.-H. Horng, IEEE J. Electron Devices Soc. **6**, 432–437 (2018).

[21]A. R. Phani, S. Santucci, S. DI Nardo, L. Lozzi, M. Passacantando, and P. Picozzi, J. Mater. Sci. **33**, 3969–3973 (1998).

[22]T. Sei, Y. Nomura, and T. Tsuchiya, J. Non-Cryst. Solids **218**, 135–138 (1997).

[23]W. Zhang, J. Zhang, Y. Li, Z. Chen, and T. Wang, Appl. Surf. Sci. **256**, 4702–4707 (2010).

[24]K.-W. Park, Y.-H. Yun, and S.-C. Choi, J. Electroceram. **17**, 263–266 (2006).

[25]I. J. Hsieh, K. T. Chu, C. F. Yu, and M. S. Feng, J. Appl. Phys. **76**, 3735–3739 (1994).

[26]I. J. Hsieh, M. S. Feng, K. T. Kuo, and P. Lin, J. Electrochem. Soc. **141**, 1617–1621 (1994).

[27]C. F. Yu and P. Lin, Jpn. J. Appl. Phys., Part 1 **35**, 5726–5729 (1996).

[28]S.-H. Yang, T.-J. Hsueh, and S.-J. Chang, J. Electrochem. Soc. **152**, H191–H195 (2005).

[29]H.-W. Choi, B.-J. Hong, S.-K. Lee, K.-H. Kim, and Y.-S. Park, J. Lumin. **126**, 359–364 (2007).

[30]O. M. Bordun, I. Yo. Kukharskyy, and V. G. Bihday, J. Appl. Spectrosc. **78**, 922–926 (2012).

[31]Y. E. Lee, D. P. Norton, and J. D. Budai, Appl. Phys. Lett. **74**, 3155–3157 (1999).

[32]Y. E. Lee, D. P. Norton, J. D. Budai, and Y. Wei, J. Appl. Phys. **90**, 3863–3866 (2001).

[33]Y. E. Lee, D. P. Norton, C. Park, and C. M. Rouleau, J. Appl. Phys. **89**, 1653–1656 (2001).

[34]S. S. Yi, I. W. Kim, J. S. Bae, B. K. Moon, S. B. Kim, and J. H. Jeong, Mater. Lett. **57**, 904–909 (2002).

[35]S. S. Yi, I. W. Kim, H. L. Park, J. S. Bae, B. K. Moon, and J. H. Jeong, J. Cryst. Growth **247**, 213–218 (2003).

[36]S. S. Yi, J. S. Bae, B. K. Moon, J. H. Jeong, I. W. Kim, and H. L. Park, Appl. Phys. A **76**, 433–437 (2003).

[37]Q. Shi, C. Wang, D. Zhang, S. Li, L. Zhang, W. Wang, and J. Zhang, Thin Solid Films **520**, 6845–6849 (2012).

[38]R.-H. Horng, C.-Y. Huang, S.-L. Ou, T.-K. Juang, and P.-L. Liu, Cryst. Growth Des. **17**, 6071–6078 (2017).

[39]T. Oshima, M. Niwa, A. Mukai, T. Nagami, T. Suyama, and A. Ohtomo, J. Cryst. Growth **386**, 190–193 (2014).

[40]A. B. Chase and J. A. Osmer, J. Am. Ceram. Soc. **50**, 325–328 (1967).

[41]P. J. M. Van Der Straten, R. Metselaar, and H. D. Jonker, J. Cryst. Growth **43**, 270–272 (1978).

[42]Z. Yan and H. Takei, J. Cryst. Growth **171**, 131–135 (1997).

[43]Z. Yan, H. Takei, and H. Kawazoe, J. Am. Ceram. Soc. **81**, 180–186 (1998).

[44]W. Jia, H. Liu, S. Huang, X. Wu, L. Lu, and W. M. Yen, J. Electrochem. Soc. **142**, 1637–1640 (1995).

[45]T. Omata, N. Ueda, K. Ueda, and H. Kawazoe, Appl. Phys. Lett. **64**, 1077–1078 (1994).

[46]See www.factsage.com for FactSage 7.2002C 2018.

[47]H. Mehling, G. Hautzinger, O. Nilsson, J. Fricke, R. Hofmann, and O. Hahn, Int. J. Thermophys. **19**, 941–949 (1998).

[48]M. G. Brik, J. Phys. Chem. Solids **71**, 1435–1442 (2010).

[49]D. K. Schroder, Semiconductor Material and Device Characterization (Wiley, New York, 1990), pp. 466–469.

[50]Z. Galazka, R. Uecker, D. Klimm, K. Irmscher, M. Naumann, M. Pietsch, A. Kwasniewski, S. Ganschow, and M. Bickermann, ECS J. Solid State Sci. Technol. **6**, Q3007–Q3011 (2017).

[51]Z. Galazka, D. Klimm, K. Irmscher, R. Uecker, M. Pietsch, R. Bertram, M. Naumann, M. Albrecht, A. Kwasniewski, R. Schewski, and M. Bickermann, Phys. Status Solidi A **212**, 1455–1460 (2015).

[52]H. S. C. O'Neill and A. Navrotsky, Am. Mineral. **68**, 181–194 (1983).

[53]L. Schwarz, Z. Galazka, T. M. Gesing, and D. Klimm, Cryst. Res. Technol. **50**, 961–966 (2015).

[54]M. Handwerg, R. Mitdank, Z. Galazka, and S. F. Fischer, Semicond. Sci. Technol. **31**, 125006 (2016).

[55]M. Lentzen, B. Jahnen, C. L. Jia, A. Thust, K. Tillmann, and K. Urban, Ultramicroscopy **92**, 233 (2002).

[56]S. Zh. Karazhanov and P. Ravindran, J. Am. Ceram. Soc. **93**, 3335–3341 (2010).

[57]H. Dixit, N. Tandon, S. Cottenier, R. Saniz, D. Lamoen, B. Partoens, V. Van Speybroeck, and M. Waroquier, New J. Phys. **13**, 063002 (2011).

[58]S. K. Sampath, D. G. Kanhere, and R. Pandey, J. Phys.: Condens. Matter **11**, 3635–3644 (1999).

[59]A. Fiedler, R. Schewski, M. Baldini, Z. Galazka, G. Wagner, M. Albrecht, and K. Irmscher, J. Appl. Phys. **122**, 165701 (2017).

[60]R. Schewski, M. Baldini, K. Irmscher, A. Fiedler, T. Markurt, B. Neuschulz, T. Remmele, T. Schulz, G. Wagner, Z. Galazka, and M. Albrecht, J. Appl. Phys. **120**, 225308 (2016).

[61]M. Albrecht, R. Schewski, K. Irmscher, Z. Galazka, T. Markurt, M. Naumann, T. Schulz, R. Uecker, R. Fornari, S. Meuret, and M. Kociak, J. Appl. Phys. **115**, 053504 (2014).

[62]F. Zerarga, A. Bouhemadou, R. Khenata, and S. Bin-Omran, Solid State Sci. **13**, 1638, 1648 (2011).

[63]L. Pisani, T. Maitra, and R. Valentí, Phys. Rev. B **73**, 205204 (2006).

[64]S. López, A. H. Romero, P. Rodríguez-Hernández, and A. Muñoz, Phys. Rev. B **79**, 214103 (2009).

[65]Y. Xia, T. Wang, X. Zhao, X. Jiao, D. Chen, J. Phys. Chem. C **122** (2018) 5509–5517

[66]S. K. Sampath and J. F. Cordaro, J. Am. Ceram. Soc. **81**, 649–654 (1998).

[67]Z. Galazka, K. Irmscher, R. Uecker, R. Bertram, M. Pietsch, A. Kwasniewski, M. Naumann, T. Schulz, R. Schewski, D. Klimm, and M. Bickermann, J. Cryst. Growth **404**, 184–191 (2014).

[68]Z. Galazka, R. Uecker, K. Irmscher, M. Albrecht, D. Klimm, M. Pietsch, M. Brutzam, R. Bertram, S. Ganschow, and R. Fornari, Cryst. Res. Technol. **45**, 1229–1236 (2010).

[69]A. V. Singh, B. Khodadadi, J. B. Mohammadi, S. Keshavarz, T. Mewes, D. S. Negi, R. Datta, Z. Galazka, R. Uecker, and A. Gupta, Adv. Mater. **29**, 1701222 (2017).